Geophys. J. Int. (2007) **171,** 613–629 doi: 10.1111/j.1365-246X.2007.03560.x

Early diagenetic greigite as a recorder of the palaeomagnetic signal in Miocene–Pliocene sedimentary rocks of the Carpathian foredeep (Romania)

Iuliana Vasiliev,[1] Mark J. Dekkers,[1] Wout Krijgsman,[1] Christine Franke,[1,2] Cor G. Langereis[1] and Tom A. T. Mullender[1]

[1]*Paleomagnetic Laboratory 'Fort Hoofddijk', Utrecht University, Budapestlaan* 17, 3584 *CD Utrecht, The Netherlands. E-mail: vasiliev@geo.uu.nl*
[2]*Department of Geosciences, University of Bremen,* PO Box 330 440, 28334 *Bremen, Germany*

Accepted 2007 July 24. Received 2007 July 23; in original form 2007 January 17

SUMMARY

During the Miocene–Pliocene, the Carpathian region represented the westernmost part of the so-called Eastern Paratethys, a palaeobioprovince that covered central and eastern Europe as well as parts of southwest Asia. Previous palaeomagnetic investigations provide a high-resolution magnetochronology for the sedimentary sequences of the Carpathian foredeep and indicate a marked transition in magnetic carriers from iron oxides to iron sulphides, in Chron C3r. Here, we demonstrate using detailed rock magnetic investigations and scanning electron microscope (SEM) analyses that the major magnetic iron sulphide mineral is greigite (Fe_3S_4). Thermomagnetic runs indicate an irreversible decrease in magnetization with increasing temperature up to 400 °C and SEM observations indicate octahedral grain morphologies and Fe:S ratios that are indicative of greigite. Hysteresis loops have 'rectangular' shapes, which are typical of single domain behaviour, with coercivity and coercivity of remanence at values of $B_c = 35$–45 mT and $B_{cr} = 52$–67 mT, respectively. First-order reversal curve diagrams have contours that close around single domain peaks with B_c values of 45–90 mT. Isothermal remanent magnetization component analysis reveals a small dispersion for the greigite component (dispersion parameter, DP ~ 0.15 log units) indicating a narrow grain size distribution. A positive fold test, inclination shallowing and two positive reversal tests are additional arguments for the syn-depositional formation of this greigite. We thus argue that (most of) the greigite was formed under early diagenetic conditions, that is, within 1000 yr of deposition of the sediment in this setting, and that it thus can be considered as a reliable recorder of the palaeomagnetic signal in this situation. The appearance of greigite during Chron C3r (between 6.0 and 5.5 Ma) in the Carpathian foredeep is most likely related to regional tectonic and/or climatic events that reshaped the basin configuration and changed the palaeoenvironmental conditions.

Key words: Carpathian foredeep, early diagenesis, greigite, iron sulphides, Paratethys, palaeomagnetism.

1 INTRODUCTION

Numerical age control of the Miocene–Pliocene sedimentary sequences of the Carpathian foredeep in Romania is mainly provided by magnetostratigraphic records (e.g. Vasiliev *et al.* 2004). Magnetostratigraphic chronologies allow age correlations between the south and east Carpathians and with Mediterranean sequences (Vasiliev *et al.* 2005). The palaeomagnetic records also indicate that a major change in magnetic properties, from mainly iron oxides to dominantly iron sulphides, took place in Chron C3r during the Lower Pontian. Palaeomagnetic directions from both types of minerals have consequently been used to better constrain the geodynamic evolution of the Carpathian arc system by determining the timing and magnitude of vertical axis rotation (Dupont-Nivet *et al.* 2005).

In an attempt to characterize the type of magnetic iron sulphide in the Carpathian sedimentary sequences, rock magnetic biplots [SIRM/χ versus coercivity for magnetic minerals and M_{rs}/M_s versus $(Bo)_{cr}/(Bo)_c$] (Peters & Dekkers 2003) were used, which indicated that monoclinic pyrrhotite is the dominant magnetic mineral (Vasiliev *et al.* 2004). Pyrrhotite would not be expected to grow during early diagenesis (Horng & Roberts 2006), which would question the reliability of the Romanian magnetostratigraphic records for detailed age correlations if the pyrrhotite had an authigenic rather than detritial origin. The magnetic properties of pyrrhotite and greigite are similar; therefore, these biplots should be used with

vigilance. Detailed rock magnetic investigations are necessary to positively identify which magnetic iron sulphide is carrying the palaeomagnetic signal in the sedimentary rocks of the Carpathian foredeep.

We present hysteresis loops, first-order reversal curve (FORC) diagrams, isothermal remanent magnetization (IRM) acquisition and backfield curves of samples from the iron sulphide-bearing rocks of the Romanian sequence in order to determine the mineral responsible for the palaeomagnetic record in these sedimentary rocks. In addition, polished sections and magnetic extracts were analysed with a scanning electron microscope (SEM). For comparison, we also investigated iron sulphide concentrates from Pliocene–Pleistocene sedimentary rocks from Taiwan whose mineralogy was previously determined by X-ray diffraction (Horng *et al.* 1992a,b, 1998). We also discuss the environmental changes that may have caused the change in magnetic mineralogy from iron oxides to iron sulphides in the Carpathian foredeep.

2 BACKGROUND

Most sediments and sedimentary rocks contain at least traces of pyrite (FeS_2) because the bulk of the world's mud is and was buried under anoxic, sulphate-reducing conditions (Berner 1984). In addition to pyrite, greigite (Fe_3S_4) is a frequent product of early diagenesis in anoxic conditions. Greigite forms in association with biogeochemical processes related to organic matter decomposition and bacterial sulphate reduction (Berner 1984; Horng *et al.* 1998). From a mass-balance viewpoint, pyrite is dominant but greigite is increasingly documented as a trace constituent in sedimentary settings (Snowball 1991; Roberts & Turner 1993; Hallam & Maher 1994; Reynolds *et al.* 1994; Roberts & Weaver 2005; Sagnotti *et al.* 2005; Rowan & Roberts 2006). Greigite and pyrrhotite are both strongly magnetic and are able to carry a stable magnetization, which makes them potentially important for palaeomagnetic studies.

The occurrence of greigite and pyrrhotite in sedimentary rocks has provoked research into their formation pathways and preservation potential. Kao *et al.* (2004) found that, compared to pyrrhotite-dominated sediments, greigite-dominated sediments have more clay, higher concentrations of reactive (cold 1 N HCl extractable) iron, higher total organic carbon (TOC) content and lower total sulphur (TS) content. Diagenetic conditions with higher Eh favour formation of greigite compared to conditions that give rise to formation of pyrrhotite (Kao *et al.* 2004). Pyrrhotite formation in sediments is less common because it is predicted to occur at pH > 11 (Hallam & Maher 1994; Weaver *et al.* 2002), which is well above the pH range expected for sedimentary pore waters. Clear documentation of the presence of monoclinic pyrrhotite in sediments suggests that these conditions have occasionally been met (Linssen 1988; Dinarès-Turell & Dekkers 1999; Weaver *et al.* 2002). In some of these studies, it has been demonstrated that authigenic pyrrhotite is late diagenetic in origin, which complicates inferences that can be made concerning its occurrence (Dinarès-Turell & Dekkers 1999; Weaver *et al.* 2002). Monoclinic pyrrhotite, however, can also record stable detrital magnetizations (Horng & Roberts 2006).

Many studies plead for early diagenetic formation of greigite (Tric *et al.* 1991; Horng *et al.* 1992b; Mary *et al.* 1993; Roberts & Turner 1993; Hallam & Maher 1994; Maher & Hallam 2005), but many others argue that caution must be exercised when considering greigite as a reliable palaeomagnetic recorder because it frequently grows during later diagenesis (Horng *et al.* 1998; Dekkers *et al.* 2000; Jiang *et al.* 2001; Roberts & Weaver 2005; Sagnotti *et al.* 2005; Rowan & Roberts 2006). Empirical observations suggest that while greigite often forms during early diagenesis, it can also form at any time during diagenesis if the necessary reactants are present (Roberts & Weaver 2005), while monoclinic pyrrhotite is generally a product of later diagenesis (Horng & Roberts 2006).

When palaeomagnetism is used to provide age constraints, that is, through magnetostratigraphy, it is of crucial importance to know whether the magnetic signal is carried by early diagenetic greigite or by late diagenetic iron sulphides. Greigite-bearing rocks could thus provide a reliable recording of the field while pyrrhotite-bearing rocks would be less prone to record an early magnetization, unless the pyrrhotite is detrital in origin.

3 GEOLOGICAL SETTING AND SECTIONS

The Carpathian foredeep of Romania formed in the Miocene in response to collision processes (Sandulescu 1988; Cloetingh *et al.* 2005). Thick sedimentary sequences were deposited in marginal basins with frequently changing environments, from marine to brackish and freshwater conditions. These fluctuations were probably imposed by changes in climate coupled with the ongoing tectonics that affected the Carpathian mountain chain. In the Miocene, the Carpathian region was the westernmost part of the Eastern Paratethys, which was an ancient bioprovince that covered central and eastern Europe plus important parts of southwest Asia. The Black Sea, Caspian Sea and Aral Lake are present-day remnants of this Paratethys water mass. Among these, the Black Sea is anomalous in the sense that it has a completely stratified water mass: it is now the largest 'poisoned' anoxic basin on Earth where, below ∼150 m, only extremophile organisms are able to live by using sulphate to oxidize organic matter (Ross & Degens 1974; Jørgensen *et al.* 2003).

The eastern Carpathian foredeep, which is located approximately 250 km west of the Black Sea (Fig. 1), contains more than 10 km of Late Miocene–Pliocene sedimentary rocks that were deposited in lacustrine to deltaic environments (Matenco 1997; Grasu *et al.* 1999; Tarapoanca 2003). Magnetostratigraphic studies of two composite sections (Putna Valley and Rîmnicu Sarat Valley) span more than 5 Myr, starting in the Upper Sarmatian (∼8 Ma) and ending in the Upper Romanian (∼2.5 Ma). The magnetostratigraphic interpretation indicates high sediment accumulation rates with a sudden increase from 0.6 to 1.55 m kyr^{-1} during Chron C3r, at around 6 Ma (Vasiliev *et al.* 2004). This increase in sedimentation rate roughly coincides with the observed change in magnetic mineralogy from iron oxides to iron sulphides (Fig. 1).

The southern Carpathian foredeep (Fig. 1) represents the sedimentary basin that developed at the contact between the South Carpathian nappe system and the Moesian Platform (Sandulescu 1984). The Late Miocene–Pliocene sedimentary succession is approximately four times thinner than in the eastern Carpathian foredeep and consists of alternating sandstones, siltstones and clays (Rabagia & Matenco 1999; Vasiliev *et al.* 2005). The magnetostratigraphy of two sections (Bădislava Valley and Topolog Valley) spans a 2.5 Myr time interval, from the upper Meotian (7 Ma) to lower Romanian (∼4 Ma) stages (Vasiliev *et al.* 2005). The carrier of the magnetization also changed from an iron oxide (in the Meotian) to an iron sulphide (in the Pontian) (Fig. 1). Note, however, that the lower Pontian is missing because of a significant hiatus between the two units (Stoica *et al.* 2007).

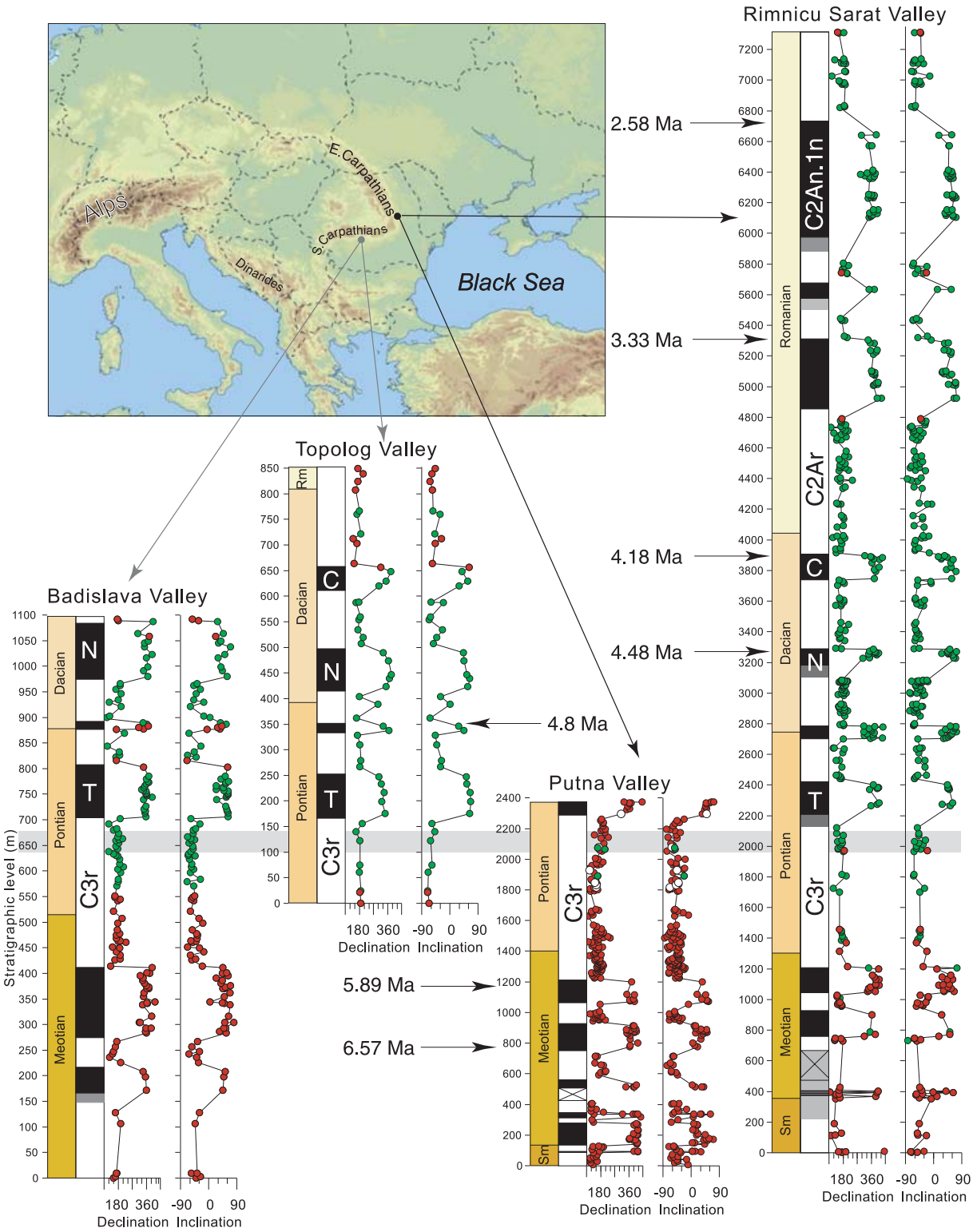

Figure 1. Map of the study areas in the Eastern Carpathian foredeep (ECF) and the Southern Carpathian foredeep (SCF). Polarity zones with palaeomagnetic data for the studied sections for the four sampled valleys: Putna and Rîmnicu Sărat from ECF and Bădislava and Topolog from SCF. Black (white) denotes normal (reversed) polarity. Ages of the most important subchrons are displayed (C = Cochiti, N = Nunivak, T = Thvera). Data are only shown for palaeomagnetic ChRM directions. Red symbols denote samples where the magnetic carrier is exclusively an iron oxide; white symbols denote samples where the magnetic signal is carried by an iron oxide, but where oxidation of an iron sulphide, most probably pyrite, also occurs; green dots indicate samples with an iron sulphide as the magnetic carrier. Next to the polarity column are represented the limits between different (local) stages of the Miocene (Sarmatian, Meotian, Pontian) and of the Pliocene (Pontian, Dacian and Romanian) according to geological maps in use (see also Vasiliev *et al*. 2004, 2005). The grey rectangle (below the Thvera subchron) indicates the approximate level of the Miocene/Pliocene boundary.

4 MATERIALS AND METHODS

Palaeomagnetic results have been previously documented for the studied sedimentary rocks (Vasiliev *et al.* 2004, 2005; Dupont-Nivet *et al.* 2005). Here, we concentrate on rock magnetic characterization of the iron sulphides that are present in the Miocene–Pliocene (<6 Ma) parts of the successions. An alternating gradient magnetometer (Princeton Measurements Corporation, MicroMag Model 2900 with 2 T magnet, noise level 2×10^{-9} Am^2) was used to successively measure hysteresis loops, FORC diagrams, IRM acquisition (after having used the demagnetization option of the MicroMag) and backfield demagnetization curves, all at room temperature. Sample masses ranged from 10 to 70 mg. Hysteresis loops were measured for 56 representative samples in order to determine the saturation magnetization (M_s), the saturation remanent magnetization (M_{rs}) and coercive force (B_c). These parameters were determined after correction for the paramagnetic contribution on a mass-specific basis. Because of the partial saturation of the pole shoes of the electromagnet, the response when measuring in-field is not linear for fields above 1.6 T. Therefore, we use the values for a maximum field of 1.6 T. To further assess the magnetic domain state, the effects of magnetic interactions, and the magnetic mineralogy, FORC diagrams were measured for the 56 representative samples. Only 51 samples yield good quality FORC diagrams. Signal-to-noise ratios were sufficient to enable use of a maximum smoothing factor (SF) of 5 (Pike *et al.* 1999); for most samples, we used SF = 3.

IRM acquisition curves were also acquired with the MicroMag system for the 51 samples for which FORC diagrams were obtained. These curves contain between 75 and 200 data points and were decomposed into coercivity components using the fitting program of Kruiver (2001). Thermomagnetic runs were measured in air with a modified horizontal translation type Curie balance with a sensitivity of approximately 5×10^{-9} Am^2 (Mullender *et al.* 1993). Approximately 30–60 mg of ~70 powdered samples were put into a quartz glass sample holder and were held in place by quartz wool; heating and cooling rates were 10 °C min^{-1}. Measurements were made up to 700 °C for 70 powdered samples from diverse lithologies. Stepwise thermomagnetic runs were also performed where samples were warmed to increasingly elevated temperatures with intermittent cooling between successive heatings. The successive temperatures were 100, 200, 300, 350, 450, 500 and 700 °C, respectively.

A resin-impregnated (semi-)polished section of representative bulk sample BD 115 (known to carry greigite) was prepared for analysis in a micro Phillips XL20 SFEG SEM, in order to validate the presence of greigite (Jiang *et al.* 2001; Roberts & Weaver 2005). Additionally, we analysed a magnetic extract (Dekkers 1988b) of the same sample (BD 115) to compare the result with that from the (semi-)polished section. The SEM was operated at 15 kV (spot size 3) in backscatter electron (BSE) detection mode. Elemental spectra were determined using energy dispersive spectroscopy (EDS). After background subtraction, the elemental composition was (semi-)quantified using the 'Remote EDS Quand Phiroz' software, version 3.4.

5 INVESTIGATION OF THE MAGNETIC CARRIERS

5.1 Hysteresis loops and FORC diagrams

Hysteresis parameters and results from FORC diagrams are compiled in Table 1. The hysteresis loops have an open form (Figs 2 a, b and d) typical of single domain magnetic behaviour. They are usually completely closed in fields of 150 mT but not yet saturated. B_c values range from 29 to 45 mT, with most values close to 40 mT. The coercivity of remanence values (B_{cr}) range from 39 to 62.5 mT with most values being between 39 and 45 mT, which is similar to those reported for greigite and monoclinic pyrrhotite (Clark 1984; Dekkers 1988a; Menyeh & O'Reilly 1991; Snowball 1991; Roberts 1995; Dekkers *et al.* 2000). The hysteresis loop in Fig. 2c remains open at comparatively high fields, indicating the presence of an additional mineral with higher coercivity. Its wasp-waisted shape indicates the co-existence of two coercivity fractions (Roberts *et al.* 1995; Tauxe *et al.* 1996). The domain state, and particularly the amount of magnetic interaction in the studied samples, emerge clearly from FORC diagrams. The FORC diagrams from the Upper Miocene–Pliocene parts of the sections (Pontian, Dacian, Romanian in terms of Paratethys stages) have contours that close around a single domain (SD) peak at B_c = 45–90 mT (usually around 55 mT) (Fig. 3), with values slightly higher than those determined from the corresponding hysteresis loops. The FORC diagrams are similar to those previously reported for greigite (Roberts *et al.* 2000, 2006; Sagnotti *et al.* 2005). The negative region in the lower left-hand quadrant (Figs 3b and c) provides additional information that single domain grains dominate the FORC distribution (Newell 2005). The central peak has considerable vertical spread and is centred below $B_u = 0$, which indicates relatively strong magnetic interaction among particles (Pike *et al*. 1999; Newell 2005). In some samples, as in Fig. 3(a), in addition to an SD peak at ~56 mT, a MD (or also possibly SP) peak at <10 mT is observed. The presence of these two peaks is a clear indication of two magnetic components.

5.2 IRM component analysis

FORC diagrams (Fig. 3) indicate that magnetic interactions are present in the Romanian Carpathian foredeep samples, which means that IRM component analysis should be used with caution and skewed-to-the-left distributions should not be given physical meaning (Egli 2004a,b; Heslop *et al.* 2004). We used the IRM fitting program of Kruiver *et al.* (2001) that is limited to symmetric distributions in the log-space (Fig. 4), which is also referred to as the cumulative log-Gaussian (CLG) approach. One sample (RM 065) was also processed with the algorithm of Egli (2004a,b), but it yielded essentially the same results under the proviso that the extra component required in the CLG approach to fit the skewed-to-the-left distribution was not interpreted as physically realistic. For sample RM 065, the CLG approach yielded: a first component with a mean acquisition field of 35.5 mT and a dispersion parameter (DP) of 0.3; a second dominant component with a mean acquisition field of 66.1 mT and a DP of 0.17; and a third component with a mean acquisition field of 158.5 mT and a DP of 0.32. The second component is interpreted as greigite. The approach of Egli (2004a,b) yielded a mean acquisition field of 69.2 mT, a DP of 0.1877 and is skewed to the left. This negative skew replaces the first low coercivity component in the CLG approach. The second coercivity component in this approach has a mean acquisition field of 164 mT, a DP of 0.262 and is slightly skewed to the right and can be assimilated with the third high coercivity component in the CLG approach. Results of the component analysis are compiled in Table 2. The preferred way of fitting the IRM acquisition curves (Fig. 4) appeared to be with a dominant coercivity component with a comparatively high mean $B_{1/2}$ ranging between ~70 and ~85 mT (Figs 4a and b) and a low dispersion (0.14–0.18 log units). The mean $B_{1/2}$ values occasionally fluctuated slightly around this range (Fig. 4c) but the dispersion remained the same. An additional coercivity component has smaller

Table 1. Magnetic minerals and domain states inferred from Curie balance and high-field magnetization measurements.

			Hysteresis parameters						FORC		
Sample code	Local stage	Minerals from Curie	B_c (mT)	B_{cr} (mT)	M_r (mAm^2 kg^{-1})	M_s (mAm^2 kg^{-1})	B_{cr}/B_c	M_r/M_s	Domain	Peak 1 (mT)	Peak 2 (mT)
Putna											
PU 009	Sm	IO	X	X	X	X	X	X	X	X	X
PU 025	Sm	IO	8.9	26.7	55.78	555.6	3.01	0.10	MD	13	X
PU 025	Sm	IO	6.9	26.0	6.683	86.89	3.79	0.08	MD	13	X
PU 034	Sm	IO									
PU 038	Sm	IO	12.2		6.205	61.49		0.10	MD	<2	X
PU 038	Sm/Me	IO	12.2	35.0	6.205	61.49	2.87	0.10	MD	<2	X
PU 041	Sm/Me	IO	7.8	25.0	5.967	74.71	3.22	0.08	MD	8	X
PU 053	Me	IO	X	X	X	X	X	X	MD	<2	X
PU 122	Me	IO	6.9	24.4	1.921	20.8	3.54	0.09	MD	<2	X
PU 126	Me	IO	6.6	23.8	0.5984	5.826	3.63	0.10	X	X	X
PU 153	Me	IO	6.1	25.5	9.121	120.8	4.18	0.08	MD	<2	X
PU 186	Po	IO	X	X	X	X	X	X	X	X	X
PU 235	Po	IO	X	X	X	X	X	X	X	X	X
PU 252	Po	IO	X	X	X	X	X	X	X	X	X
PU 260	Po	IS	35.6	29.8	1.62	12.36	0.84	0.13	SD	X	53
PU 261	Po	IO+IS	12.6	29.8	0.1929	1.442	2.37	0.13	MD	8	X
PU 272	Po	IO+IS	X	X	X	X	X	X	X	X	X
PU 297	Po	IO	7.1	22.6	1.289	9.493	3.19	0.14	MD	7	X
PU 308	Po	IO	6.8	25.0	1.577	17.49	3.68	0.09	MD	<2	X
Rimnicu Sarat											
RM 003	Sm	IO+IS	X	X	X	X	X	X	X	X	X
RM 011	Sm	IO+IS	X	X	X	X	X	X	X	X	X
RM 013	Sm	IO	6.1	23.9	1.157	23.14	3.89	0.05	MD	~5	X
RM 014	Sm	IO+IS	X	X	X	X	X	X	X	X	X
RM 019	Me 1	IO+IS	X	X	X	X	X	X	X	X	X
RM 021	Me 1	IS+IO	10.9	29.9	0.3342	9.998	2.74	0.03	MD	>2	X
RM 025	Me 2	IO	8.0	28.7	2.992	42.29	3.58	0.07	MD	>2	X
RM 028	Me 2	IO	X	X	X	X	X	X	X	X	X
RM 039	Me/Po	IS	39.8	55.2	8.397	24.28	1.39	0.35	SD	X	49
RM 043	Po	IS+IO	21.2	49.5	0.9129	12.11	2.33	0.08	SD	X	42
RM 045	Po	IS	38.5	58.6	3.076	12.59	1.52	0.24	SD	X	50
RM 051	Po	IS+IO	X	47.9	X	X	X	X	MD+SD	>2	51
RM 051	Po	IS+IO	28.8	X	0.8743	8.13	X	0.11	X	X	X
RM 051	Po	IS+IO	28.6	58.9	0.773	7.344	2.06	0.11	MD+SD	>2	50
RM 053	Po	IS+IO	29.2		0.8927	11.07		0.08	MD+SD	>2	56
RM 056	Po	IO+IS	32.3	55.7	0.4086	1.655	1.72	0.25	MD+SD	>2	50
RM 065	Po	IS	30.6	52.1	1.329	8.069	1.70	0.16	SD	X	35
RM 065.B	Po	IS	28.4	46.0	4.514	19.29	1.62	0.23	SD	X	38
RM 065	Po	IS	20.7		2.995	22.21		0.13	X	X	X
RM 078	Po/Dc	IS	39.2	55.8	23.49	64.45	1.43	0.36	SD	X	54
RM 100	Dc 1	IS+IO	16.0	63.3	0.2734	10.25	3.96	0.03	too noisy	X	X
RM 100	Dc 1	IS+IO	X	63.2	X	X	X	X	too noisy	X	X
RM 172	Dc 1	IS	39.2	52.8	0.6257	2.082	1.35	0.30	MD+SD	>2	55

Table 1. (*Continued.*)

			Hysteresis parameters						FORC		
Sample code	Local stage	Minerals from Curie	B_c (mT)	B_{cr} (mT)	M_r (mAm^2 kg^{-1})	M_s (mAm^2 kg^{-1})	B_{cr}/B_c	M_r/M_s	Domain	Peak 1 (mT)	Peak 2 (mT)
RM 146	Dc 2	IS+IO	39.6	53.1	2.32	4.75	1.34	0.49	SD	X	49
RM 146	Dc 2	IS+IO	39.6	55.5	4.957	15.1	1.40	0.33	SD	X	52
RM 131	Dc/Rm	IS+IO	X	X	X	X	X	X	X	X	X
RR 025	Rm 1	IS+IO	30.7	43.8	47.05	105	1.43	0.45	SD	X	38
RR 039	Rm 1	IO+IS	X	X	X	X	X	X	X	X	X
RR 062	Rm 1	IO+IS	11.8	38.7	0.6215	11.39	3.29	0.05	MD	12	X
RR 070	Rm 1	IO+IS	14.0	48.9	0.6074	12.35	3.48	0.05	MD	13	X
RR 087	Rm 1	IO	15.1	47.0	0.4456	9.995	3.12	0.04	X	X	X
RR 104	Rm 1	IS	104.7	118.9	222.6	390.1	1.14	0.57	SD	X	90
RR 111	Rm 2	IO+IS	12.7	49.2	0.2967	10.49	3.87	0.03	too noisy	X	X
RR 122	Rm 2	IS	27.7	62.4	1.738	11.46	2.25	0.15	SD	X	60
RR 130	Rm 2	IS+?IO	9.4	X	0.3607	9.157	X	0.04	too noisy	X	X
RR 131	Rm 2	IO	X	X	X	X	X	X	X	X	X
Badislava											
BD 017	Me	IO	11.2	49.4	0.2952	7.905	4.43	0.04	MD	10	X
BD 035	Me	IO	9.2	30.1	0.9183	18.68	3.28	0.05	MD	8	X
BD 042	Me	IO	12.6	63.8	0.5401	6.457	5.07	0.08	MD	<2	X
BD 050	Me	IO	8.6	26.9	1.972	27.37	3.13	0.07	MD	8	X
BD 084	Me/Po	IO+IS	21.1	67.3	1.364	5.396	3.19	0.25	MD+SD	<2	68
BD 098	Po	IS	X	X	X	X	X	X	X	X	X
BD 101	Po	IS	46.3	66.9	1.696	60908	1.44	0.25	SD	X	63
BD 115	Po	IS	42.4	57.6	35.54	84.54	1.36	0.42	SD	X	52
BD 118	Po	IS	45.6	62.5	4.417	15.86	1.37	0.28	SD	X	57
BD 120	Po	IS+IO	33.0	53.8	3.461	19.57	1.63	0.18	SD	X	47
B 09	Po	IO	9.1	29.4	2.385	26.88	3.23	0.09	MD	<2	X
B 10	Po	IO+IS	X	X	X	X	X	X	PSD?	12	X
B 13	Po/Dc	IO+IS	18.1	33.5	3.788	21.32	1.85	0.18	MD+SD	13	60
B 20	Dc	IO	18.0	31.2	2.304	15.32	1.73	0.15	SD	11	X
B 25	Dc	IO+IS	28.5	51.3	3.264	15	1.80	0.22	MD+SD	8	57
B 36	Dc	IO+IS	14.4	19.1	1.941	18.2	1.32	0.11	SD	10	X
B 40	Dc	X	13.7	19.1	1.154	12.93	1.39	0.09	SD	10	X
B 42	Dc	X	18.9	42.1	2.361	16.68	2.23	0.14	MD+SD	10	70
Topolog											
TP 18	Po	IO+IS	9.8	46.9	0.5868	14	4.79	0.04	X	X	X
TP 20	Po	IS	35.0	69.4	1.13	11.07	1.98	0.10	SD	X	64
TP 22	Po	IS	39.4	65.6	1.76	10.74	1.66	0.16	SD	X	62
TP 30	Dc	IO	7.2	36.6	0.2253	12.25	5.11	0.02	MD	<2	X
TP 57	Dc	IS	39.1	54.9	7.319	24.37	1.41	0.30	SD	X	49
TP 57	Dc	IS	40.4	58.4	14.15	44.83	1.45	0.32	SD	X	49
TP 61	Rm	IO	9.6	39.8	0.4722	11.98	4.17	0.04	MD	<2	X
Taiwan											
TWM 14	Pliocene	X	21.5	60.0	401.1	1670	2.79	0.24	MD+SD	<2	60
TWM 17	Pliocene	X	46.2	66.6	4637	10830	1.44	0.43	SD	X	62

Notes: Sm: Sarmatian, Me: Meotian, Po: Pontian, Dc: Dacian and Rm: Romanian. IO: iron oxide, IS: iron sulphide (including pyrite). SD: single domain, MD: multidomain, PSD = pseudo-single domain.

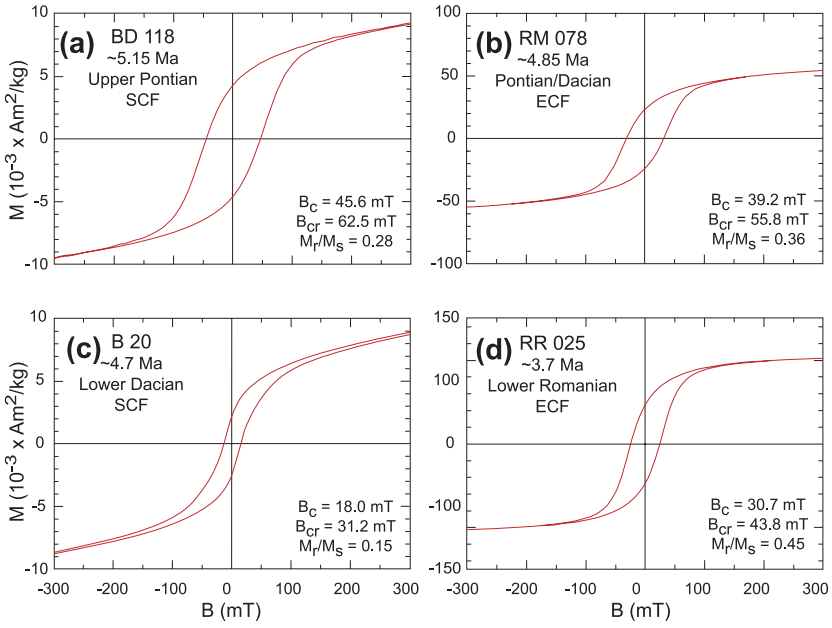

Figure 2. Hysteresis loops for characteristic samples from the Carpathian foredeep. The central parts of the loops are shown up to ±300 mT. The loops are displayed after paramagnetic slope correction on a mass-specific basis. The age and stage of the sedimentary rocks is indicated on the upper left-hand side of each panel. Hysteresis parameters are listed on the lower right-hand corner of each panel.

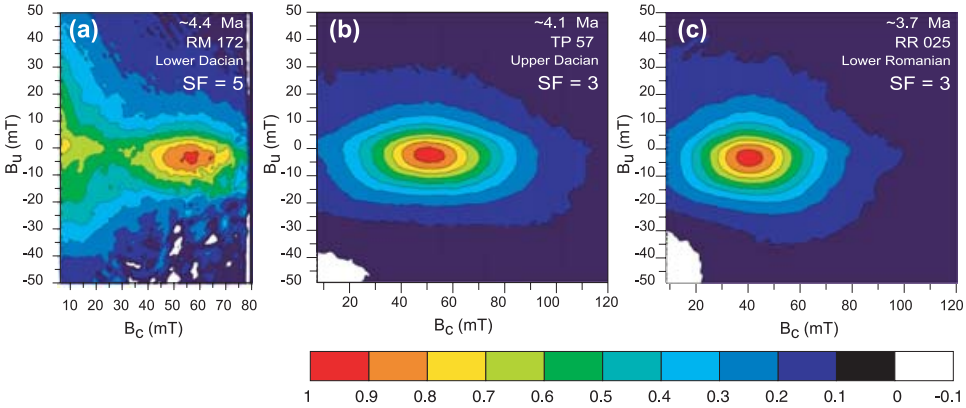

Figure 3. Representative FORC diagrams for three samples from the Carpathian foredeep. Each FORC distribution contains 10 contours. The scale indicates the density of the FORC distribution. In the upper right-hand corner are listed the sample code, age and stage of the sedimentary rocks and the applied smoothing factor (see Pike *et al*. 1999; Roberts *et al*. 2000).

values for $B_{1/2,}$ usually between ∼24 and ∼35 mT. This component has no physical meaning in the majority of cases. In several cases, the low coercivity component could be physically interpreted: hysteresis loops and FORC diagrams (e.g. Fig. 3a) indicated the existence of an extra low coercivity component in those samples. A higher coercivity component is also present, but it generally has a small magnetization contribution (<10 per cent, but rarely up to 27 per cent). The $B_{1/2}$ for this component range is loosely defined between 125 mT and almost 2 T, which could represent maghemitized magnetite, hematite, goethite or any combination of these. To define the exact mineralogy of this high coercivity component is beyond the scope of this paper.

5.3 Thermomagnetic runs

In thermomagnetic runs of bulk sedimentary rock samples, the paramagnetic component is dominant for almost all samples, as indicated by the hyperbolic shape of the curves (Fig. 5). A summary of the thermomagnetic results is shown in Table 1; below we describe their essence. Typical results for >90 per cent of the samples from the younger parts of the sections indicate an irreversible decrease in magnetization up to ∼410–420 °C (Figs 5b–d). A clearly steeper decrease in magnetization slope is detectable at around 250 °C (Figs 5c and d). This is most likely caused by greigite because of its irreversible decrease in magnetization between 200 and 400 °C (Krs *et al.* 1992; Reynolds *et al.* 1994; Roberts 1995; Dekkers *et al.* 2000).

At 415–420 °C the magnetization increases in some samples because of the creation of a new magnetic mineral that forms at the expense of iron sulphides. The increase is interpreted to be caused by greigite degradation (Krs *et al.* 1992) combined with pyrite oxidation, which occurs over approximately the same temperature range (Passier *et al.* 2001). New production of magnetite is a likely cause of aberrant NRM behaviour observed during thermal

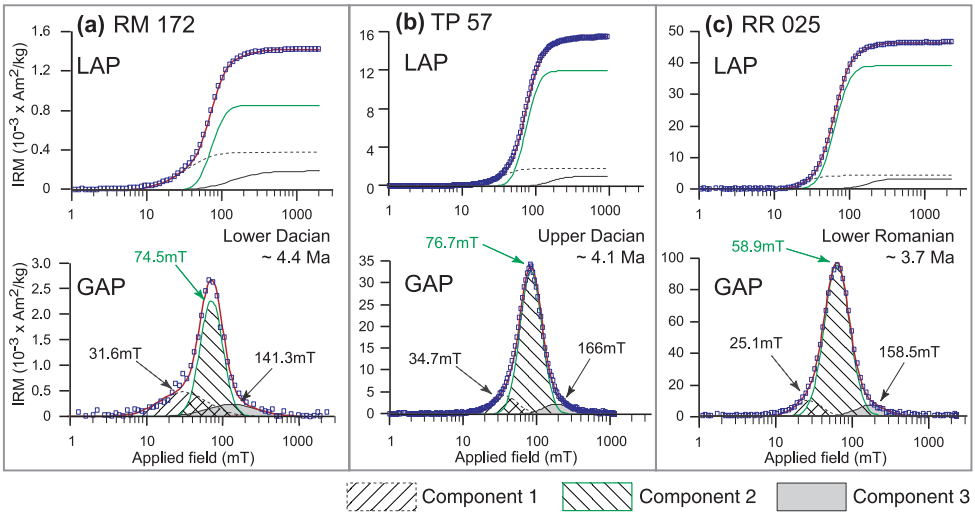

Figure 4. Representative examples of the IRM component analysis (Kruiver *et al*. 2001). Squares are measured data points. The components are marked with different lines in: the linear acquisition plot (LAP) and with different cross-hatches/shades in the gradient acquisition plot (GAP). Component 1 has a low coercivity, component 2 has higher coercivity and component 3 has the highest coercivity. IRM is in $Am^2\ kg^{-1}$, $\log_{10}$ ($B_{1/2}$) and DP are in $\log_{10}$ mT. Values of $B_{1/2}$ are displayed in each panel.

demagnetization at $T > 400\ ^\circ$C (see also Vasiliev *et al*. 2004, 2005). Magnetite continues to be produced until 500 °C. At higher temperatures it oxidizes to hematite (much lower magnetization is observed in the cooling segment after heating to 700 °C). Generally, most of the magnetic material (both original and produced during the experiment) was consumed by heating to 580–590 °C, although a ferrimagnetic signal sometimes continues to be present up to 620–630 °C, which indicates the presence of maghemite (either originally present in the sample or a product of oxidation during the thermomagnetic run).

In sample PU 261 (Fig. 5a), a small increase in magnetization is observed after heating above ∼300 °C before the larger increase at 415–420 °C. The total magnetization is higher than for the paramagnetic contribution (inferred from the final cooling curve) unlike that in Figs 5b–d. Therefore, the magnetic mineralogy in sample PU 261 appears to be subtly different from that of the other samples. The original magnetic material is interpreted to be an iron oxide that is accompanied by pyrite that upon heating transforms to magnetite. The low coercivity component in a wasp-waisted hysteresis loop for this sample supports this interpretation; the loop is closed at ±150 mT, which is typical of multidomain magnetite (see parameters in Table 1). This situation occurs in <10 per cent of the analysed samples from the younger parts of the sections. Such samples are indicated by white circles in Fig. 1, which represent sites where an iron oxide is the magnetic carrier. An important quantity of pyrite is indicated by the alteration at ∼420 °C, which indicates that reducing conditions existed in the sedimentary environment.

5.4 SEM observations

Thermomagnetic measurements strongly suggest that the iron sulphide from the Carpathian foredeep is greigite, but rock magnetic biplots of Peters & Dekkers (2003) point to pyrrhotite. We therefore, further test this interpretation with SEM analysis.

The SEM observations from the unpolished section and the magnetic extract both indicate the presence of fine-grained iron sulphides (<500 nm) (Figs 6 and 7). Semi-quantitative EDS analysis enables us to distinguish between the specific Fe:S ratios of different iron sulphide minerals. The iron–sulphur ratio for greigite (Fe_3S_4 ∼43 per cent:57 per cent) is close to that of pyrrhotite (Fe_7S_8 ∼46 per cent:52 per cent), but all of the iron sulphides in our samples were positively identified as either greigite (Figs 6, 7a and b) or pyrite (Figs 7c and d).

Iron sulphide minerals can also be distinguished by their distinct morphologies: pyrrhotite is typically platy (Weaver *et al.* 2002), while greigite and pyrite occur as octahedral grains (Roberts & Weaver 2005). The latter morphology is clearly visible in Fig. 6 and the X-ray spectra provide the correct Fe:S ratio for greigite (Figs 6 and 7b). The SEM observations, therefore, clearly indicate the presence of fine-grained greigite in our samples. The greigite grains have a darker contrast than pyrite, probably because it is less well polished with surfaces that scatter electrons compared to the smoother surfaces of the pyrite grains (Jiang *et al.* 2001; Roberts & Weaver 2005).

6 DISCUSSION

6.1 Greigite in the Miocene–Pliocene sedimentary rocks of the Carpathian foredeep

Conventional rock magnetic properties indicate that the magnetic carrier in the majority of the Pliocene samples from the Romanian Carpathian foredeep is an iron sulphide mineral (Vasiliev *et al*. 2004, 2005). Our thermomagnetic measurements and SEM observations clearly demonstrate that greigite is the main magnetic mineral in these sedimentary rocks. The palaeomagnetic signal from these greigite-bearing sequences is considered to be palaeomagnetically reliable for four main reasons.

1. The palaeomagnetic directions are consistent after tilt corrections (bedding tilts vary from 90° to 20°). We performed the fold test of Tauxe & Watson (1994) on the data from the Rîmnicu Sărat section, which proved to be positive (Fig. 8a), indicating that the magnetization was acquired before tilting of the strata.
2. In the eastern Carpathian sections, the characteristic remanent magnetization (ChRM) could be easily distinguished from

Table 2. Results of IRM component analysis for the studied Carpathian foredeep samples. Component contributions are given as percentages

			Component 1					Component 2					Component 3				
Sample code	Local stage	Level (in m)	Contribution (per cent)	SIRM	log($B_{1/2}$)	$B_{1/2}$	±DP	Contribution (per cent)	SIRM	log($B_{1/2}$)	$B_{1/2}$	±DP	Contribution (per cent)	SIRM	log($B_{1/2}$)	$B_{1/2}$	±DP
Putna																	
PU 025	Sm	124.2	23.6	135	1.25	17.8	0.33	76.4	438	1.62	41.7	0.24	X	X	X	X	X
PU 038	Sm/Me	176.7	23.8	45	1.3	20	0.35	66.1	125	1.69	49	0.29	10.1	19	2.8	361	0.3
PU 041	Sm/Me	182.7	16.9	27	1.2	15.8	0.5	80	128	1.55	35.5	0.3	3.1	5	3.2	1584.9	0.5
PU 053	Me	260.3	22.6	40	1.16	14.5	0.4	76.3	135	1.63	42.2	0.27	1.1	2	2.15	141.3	0.25
PU 122	Me	901.2	35.1	26	1.4	25.1	0.5	64.9	48	1.6	37.4	0.28	X	X	X	X	X
PU 126	Me	933.5	8.8	1.3	1	10	0.4	86.2	12.8	1.55	35.5	0.3	5.1	7.5	2.5	316.2	0.65
PU 153	Me	1364.5	17	15	1.2	15.8	0.42	81.8	72	1.6	39.8	0.29	1.1	1	2.25	177.8	0.32
PU 261	Po	1860.9	10.2	2	1.15	14.1	0.5	87.3	17.2	1.68	47.9	0.37	2.5	5	3.3	1995.3	0.3
PU 297	Po	2210.5	22.3	10	1.3	20	0.5	75.7	34	1.55	35.5	0.3	2	0.9	3.1	1258.9	0.5
PU 308	Po	2335	24.4	4	1.2	15.8	0.3	73.2	12	1.6	39.8	0.28	2.4	0.4	2.4	251.2	0.37
Rimnicu Sarat																	
RM 013	Sm	408.4	10.6	1.6	1.29	19.5	0.6	89.4	13.5	1.62	41.7	0.33	X	X	X	X	X
RM 021	Me 1	900	X	X	X	X	X	99.7	0.35	1.59	38.9	0.29	0.3	0.001	2.3	199.5	0.37
RM 025	Me 2	1027.5	8.1	0.25	0.9	7.9	0.35	87.9	2.7	1.62	41.2	0.27	3.9	0.12	2.3	199.5	0.25
RM 039	Me/Po	1413	18.8	15	1.61	40.7	0.19	72.5	58	1.87	74.1	0.14	8.8	7	2.2	158.5	0.29
RM 043	Po	1699	15.6	1.4	1.35	22.4	0.3	74.4	6.7	1.78	59.6	0.16	10	0.9	2.25	177.8	0.3
RM 045	Po	1807	11.9	3.7	1.42	26.3	0.28	78.5	24.5	1.87	74.1	0.16	9.6	3	2.3	199.5	0.28
RM 051	Po	1998	24.1	1.85	1.45	28.2	0.32	60.9	4.68	1.87	74.1	0.16	15	1.15	1.95	89.1	0.5
RM 056	Po	2246	28.8	6	1.4	25.1	0.33	62.5	13	1.91	81.3	0.18	8.7	1.8	2.25	177.8	0.35
RM 065	Po	2454	24	23	1.55	35.5	0.3	66.7	64	1.82	66.1	0.17	9.4	9	2.2	158.5	0.32
RM 078	Po/Dc	2735	12.7	32	1.55	35.5	0.28	75.3	189	1.85	70.8	0.14	12	30	2.1	125.9	0.3
RM 146	Dc 2	3896.5	16	16	1.55	35.5	0.3	75	75	1.83	67.6	0.16	9	9	2.2	158.5	0.3
RM 172	Dc 1	3449	26.8	3.8	1.5	31.6	0.32	59.9	8.5	1.87	74.5	0.16	13.4	1.9	2.15	141.3	0.32
RR 025	Rm 1	4688.3	9.1	42	1.4	25.1	0.17	84.1	390	1.77	58.9	0.16	6.9	32	2.2	158.5	0.18
RR 062	Rm 1	5313.8	69	4.35	1.73	53.7	0.32	25.4	1.6	1.3	20	0.31	5.6	0.35	2.25	177.8	0.3
RR 070	Rm 1	5741.7	1.7	0.1	1.1	12.6	0.3	72.4	4.2	1.65	44.7	0.28	25.9	1.5	2.5	316.2	0.4
RR 087	Rm 1	6232.9	6.7	0.3	1.2	15.8	0.3	80	3.6	1.65	44.7	0.32	13.3	0.6	2.67	467.7	0.32
RR 104	Rm 1	6404.1	11.7	260	2	100	0.3	67.3	1500	2.7	117.5	0.17	21.1	470	2.4	251.2	0.29
RR 122	Rm 2	7057	16.6	2.9	1.52	33.1	0.3	71.6	12.5	1.88	75	0.14	11.7	2.05	2.25	177.8	0.3
Badislava																	
BD 017	Me	247.23	12.4	0.6	1.1	12.6	0.5	51.5	2.5	1.61	40.7	0.34	36.1	1.75	2.35	332.9	0.4
BD 035	Me	344.18	10.8	1	1	10	0.3	84.3	7.8	1.62	41.7	0.29	4.9	0.45	2.65	446.7	0.28
BD 042	Me	375.62	21.3	0.95	1.25	17.8	0.37	52.6	2.35	1.81	64.6	0.33	26.2	1.71	2.67	467.7	0.37
BD 050	Me	401.29	19.6	4	1.2	15.8	0.25	73.5	15	1.61	40.7	0.22	6.9	1.4	2.2	158.5	0.3
BD 084	Me/Po	570.06	34.5	3.8	1.56	36.3	0.31	55.5	6.1	1.97	93.3	0.15	10	1.1	2.39	245.5	0.3
BD 101	Po	658.90	15.3	0.45	1.6	39.8	0.32	75.5	2.22	1.92	83.2	0.14	9.2	0.27	2.25	177.8	0.3
BD 115	Po	712.82	14.7	50	1.6	39.8	0.28	72.7	248	1.88	75.9	0.14	12.6	43	2.2	158.5	0.3
BD 118	Po	725.95	15.9	7	1.56	36.3	0.3	72.7	32	1.9	79.4	0.14	11.4	5	2.2	158.5	0.35
BD 120	Po	743.78	19.5	6.5	1.55	35.5	0.25	72.1	24	1.9	79.4	0.16	84	2.8	2.3	199.5	0.3

Table 2. (*Continued.*)

			Component 1					Component 2					Component 3				
Sample code	Local stage	Level (in m)	Contribution (per cent)	SIRM	$\log(B_{1/2})$	$B_{1/2}$	±DP	Contribution (per cent)	SIRM	$\log(B_{1/2})$	$B_{1/2}$	±DP	Contribution (per cent)	SIRM	$\log(B_{1/2})$	$B_{1/2}$	±DP
B 09	Po	876.35	20.3	4.4	1.2	15.8	0.3	70.5	15.3	1.61	40.7	0.3	9.2	2	2.5	316.2	0.4
B 13	Po/Dc	886.48	60.5	23	1.38	24	0.3	28.9	11	1.95	89	0.16	10.5	4	2.3	199.5	0.35
B 20	Dc	934.27	26.8	6.3	1.92	83.2	0.15	63.3	14.9	1.39	24.5	0.32	10	2.35	2.4	251.2	0.3
B 25	Dc	969.13	43.8	14.4	1.43	26.9	0.33	48.6	16	1.9	79.4	0.15	7.6	2.5	2.3	199.5	0.35
B 36	Dc	1041.28	5.2	0.85	0.9	7.9	0.3	86.2	14	1.38	24	0.31	8.6	1.4	2.3	199.5	0.31
B 40	Dc	1058.17	X	X	X	X	X	85.6	10.1	1.34	21.9	0.29	14.4	1.7	2.25	177.8	0.35
B 42	Dc	1073.63	54.1	12.5	1.34	21.9	0.29	32.5	7.5	1.93	85.1	0.17	13.4	3.1	2.4	251.2	0.3
Topolog																	
TP 18	Po	327.97	36.1	2.2	1.39	24.5	0.31	55.7	3.4	1.8	75	0.18	8.2	0.5	2.3	199.5	0.4
TP 20	Po	345.86	7.2	0.7	1.52	33.1	0.37	82.5	8	1.93	85.1	0.17	10.3	1	2.3	199.5	0.35
TP 30	Dc	463.15	18.9	0.2	1	10	0.32	66	0.7	1.68	47.9	0.32	15.1	0.16	2.6	398.1	0.35
TP 57	Dc	766.63	11.1	18	1.54	34.7	0.17	73.5	119	1.89	76.7	0.15	6.2	10	2.22	166	0.17
TP 61	Rm	838.76	12.2	0.5	1	10	0.32	63.4	2.6	1.59	38.9	0.29	24.4	1	2.3	199.5	0.38
Taiwan																	
TWM 14	Pliocene	327.97	40.7	8000	1.59	38.9	0.34	41.1	8090	1.9	79.4	0.13	18.2	3570	2.2	158.5	0.32
TWM 17	Pliocene	345.86	8.2	3760	1.5	31.6	0.2	79.4	36500	1.9	78.5	0.14	12.4	5720	2.23	169.8	0.18

Notes: SIRM is in 10^{-3} Am^2kg^{-1}, $B_{1/2}$ and DP are in $\log_{10}$ mT, $B_{1/2}$ in mT. See Table 1 for abbreviations. All components identified for all samples are reported except for sample TP 57 where a fourth component was found with a relative contribution of 9.3 per cent.

viscous and/or secondary NRMs because of the large dip of the strata (Vasiliev *et al.* 2004). In the Putna Valley section the dip was too uniform to allow application of the fold test.

3. Inclination error affected palaeomagnetic directions from these sedimentary rocks (Dupont-Nivet *et al.* 2005). Applying the correction method for inclination error using the field model TK03.GAD (Krijgsman & Tauxe 2004; Tauxe & Kent 2004), we observed that palaeomagnetic directions are significantly flattened (Figs 8b and c). For the Bădislava section, the mean observed inclination is 50.5°, while the corrected inclination is 69.9° (Fig. 8b). For Rîmnicu Sărat, the mean observed inclination is 52.5° while the corrected inclination is 66.6° (Fig. 8c). The corrected mean inclinations are within error (95 per cent bootstrap) of the expected inclination for the studied sites (63.8°) during the Pliocene, whereas the recorded inclinations are significantly lower. We interpret the shallow inclination to result from inclination shallowing during deposition and compaction, which suggests that the magnetization directions were acquired before compaction, that is, in an early stage after deposition.

4. In all sections, normal and reversed polarities are documented in a stratigraphically coherent sense, which straightforwardly correlate to the geomagnetic polarity time scale (Fig. 1). Moreover, the calculated values for the average duration of observed sedimentary cycles are close to the average duration of a precession cycle (21.7 kyr) and indicate that the sedimentary cycles are astronomically forced (Vasiliev *et al.* 2004).

Because of the potential problem associated with the reliability of the magnetostratigraphic records obtained from iron sulphides, we applied the reversal test of McFadden & McElhinny (1990) on exclusively iron sulphide-bearing ChRM data from Bădislava, Topolog and Rîmnicu Sărat (the green dots in Fig. 1). For the Bădislava section, the reversal test is positive (classification B) (left-hand side of Fig. 8d). The Topolog section provided a positive reversal test as well (classification C—not shown). The reversal test is negative for the Rîmnicu Sărat section (right-hand side of Fig. 8d). We suspect that this is caused by the presence of an un-removed secondary NRM component. Most likely, this secondary NRM direction is a present-day overprint since the distribution of both normal and reversed polarity directions are dragged towards the geocentric actual dipole field direction in tilt-corrected coordinates (Fig. 8d). The removal of this secondary NRM component was successful for Bădislava and Topolog because we applied more suitable (smaller) demagnetization steps, with a focus on the lower temperature interval (between 210 and 340 °C). This case demonstrates the importance of using sufficiently small demagnetization steps to enable isolation of a ChRM in iron sulphide bearing sediments. Nevertheless, all evidence is consistent with early diagenetic formation of the greigite and thus for an early, syn-depositional NRM acquisition. We therefore, conclude that the greigite in the sedimentary rocks from the Carpathian foredeep is a reliable recorder of a syn-depositional palaeomagnetic signal.

Kao *et al*. (2004) demonstrated that diagenetic environments with low TS to reactive iron ratios support the formation and preservation of greigite. TOC and reactive iron contents are highest in greigite-bearing sediments from Taiwan (Kao *et al.* 2004), which also tend to be finer-grained. Kao *et al.* (2004) suggest that lower labile organic matter concentrations, due to high sedimentation rates that also coincided with higher reactive (ferric) iron availability, would favour greigite formation over formation of pyrite or pyrrhotite. These conditions were probably also met in the Romanian Carpathian foredeep, and, as suggested by palaeomagnetic field tests, the

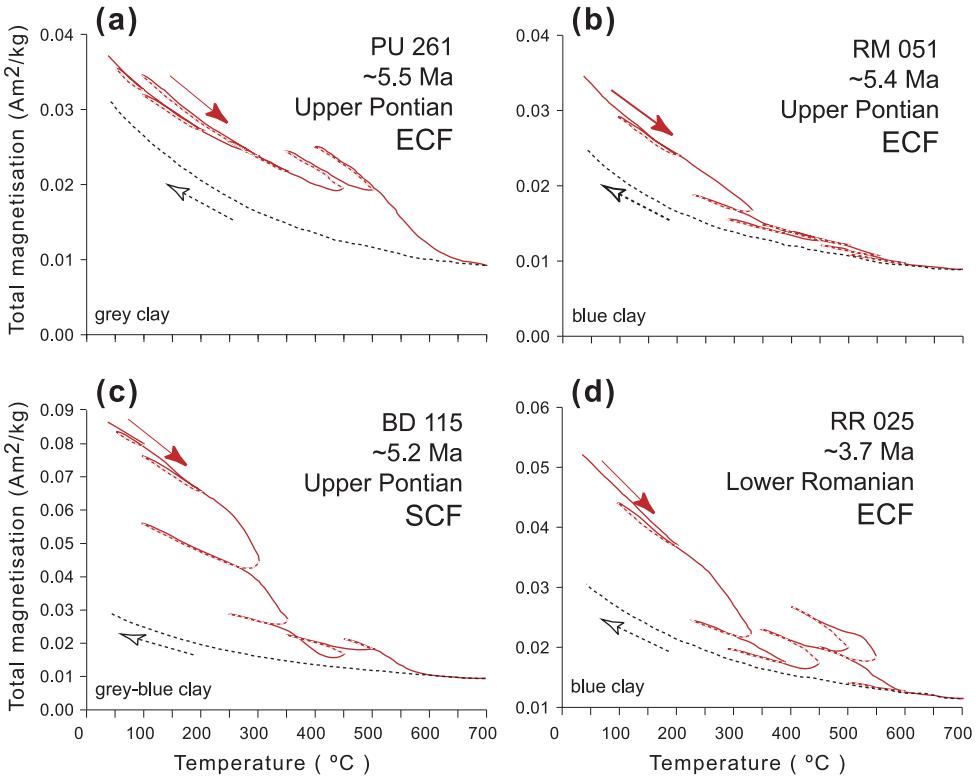

Figure 5. Representative thermomagnetic runs for samples during different heating (solid lines) and cooling (dashed lines) runs that were performed at a rate of 10 °C min^{-1}. The total magnetization is plotted in a series of runs to increasingly higher temperatures. Arrows refer to heating and cooling segments, respectively. Measurements were made every six seconds, which is equivalent to one every degree Celsius. The applied cycling field varied between 150 and 300 mT. In the upper right-hand corner are the approximate age and the stage corresponding to each sample. An increase in the total magnetization starting at 300 °C is evident in panel (a), indicating newly formed magnetic minerals, although the original magnetic material does not seem to have been affected. In (b), (c) and (d) an increase in the total magnetization starts at 410–416 °C indicating the formation of new magnetic minerals because of oxidation of an iron sulphide (either magnetic or not magnetic).

greigite was formed during latest Miocene to Pliocene times and has been preserved until today. Lower sulphate concentrations typical of brackish waters would also favour formation of greigite rather than pyrite or pyrrhotite because dissolved pore water sulphide concentrations under anoxic conditions will be lower than in open marine settings.

6.2 Comparison with greigite from southwest Taiwan

To compare the magnetic properties of the studied greigite samples with other samples known to contain greigite, we also applied the same set of rock magnetic analyses to greigite concentrates from Pliocene sediments from Taiwan (TWM 14 and TWM 17 from Horng *et al*. 1992a,b, 1998). The magnetic mineralogy was previously determined by X-ray diffraction, which revealed that sample TWM 14 contains greigite, accompanied by minor pyrrhotite and magnetite, respectively. Sample TWM 17 has greigite as the main magnetic mineral, although some magnetite was also detected (Horng *et al.* 1992a).

The hysteresis loop for sample TWM 14 (Fig. 9a) has a similar shape and hysteresis parameters as sample BD 084 (Fig. 9c) from the southern Carpathian foredeep. The hysteresis loop for sample RM 051 has a higher paramagnetic contribution (Fig. 9b) but coercivity values are similar. The FORC distribution for sample TWM 14 (Fig. 9d) has two maxima, one at $B_c < 10$ mT and one around a SD peak at $B_c \sim 60$ mT. This indicates the presence of two coercivity fractions. Similar behaviour is observed for some samples from the Carpathian foredeep (Figs 9e and f, Fig. 3a), although the concentration of magnetic minerals is less in the latter. IRM component analysis for samples TWM 14, RM 051, BD 084 (Figs 9g and i) is similar. In sample TWM 14 there are two main components: one with a high $B_{1/2}$ of 79.4 mT and a low DP of 0.13 (log units) and a second important component with a lower $B_{1/2}$ of 38.9 mT and a higher dispersion DP of 0.34 (log units). This latter component has no physical meaning; it likely arises from larger magnetic interaction in the concentrate. There is a third component with a higher DP of 0.32 and high $B_{1/2} = 158.5$ mT, which is compatible with fine-grained hematite. This might be a consequence of partial oxidation (samples were stored for more than 10 yr) despite storage in a desiccator with silica gel to maintain a dry atmosphere.

The hysteresis loop for sample TWM 17 (Fig. 10a) has a square SD shape with parameter values close to that of Figs 10b and c, which resembles parameters for a large number of other samples (Table 2). In the FORC diagram for sample TWM 17 (Fig. 10d) (see also Roberts *et al.* 2006), the contours are centred on a SD maximum at $B_c = 62$ mT. This FORC distribution is almost identical to that for sample RR 122 (Fig. 10f), where the contours centre on a SD peak at $B_c = 60$ mT. The SD peak can also be observed in BD 115 (Fig. 10e), but it has a slightly lower coercivity value of $B_c = 54$ mT. In all three FORC diagrams in Fig. 10, there is a fairly wide distribution of contour density with respect to B_u, which is centred below $B_u = 0$, which indicates relatively strong magnetic interactions among particles (Pike *et al.* 1999; Roberts *et al.* 2000, 2006; Rowan & Roberts 2006). IRM component analysis

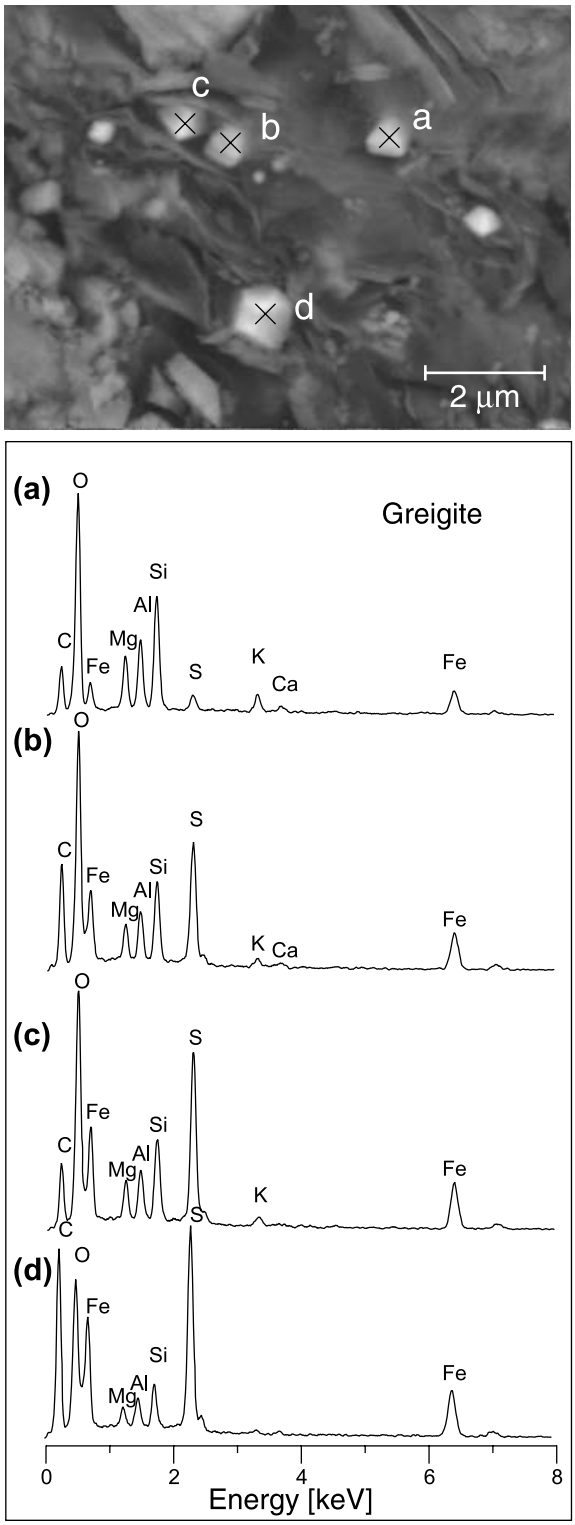

Figure 6. Backscattered electron micrograph of an unpolished cut section of sample BD115. Individual octahedral greigite particles (a–d) are 1 μm maximum in size. The respective labelled and equally scaled elemental spectra are shown below. A cross on the micrograph marks the exact position of each EDS analysis. The mineral phases were identified by automated semi-quantification of the EDS. Mg, Al, Si, K and potentially Ca content in the elemental spectra are due to the background signal. The C peak originates from the carbon coating of the sample.

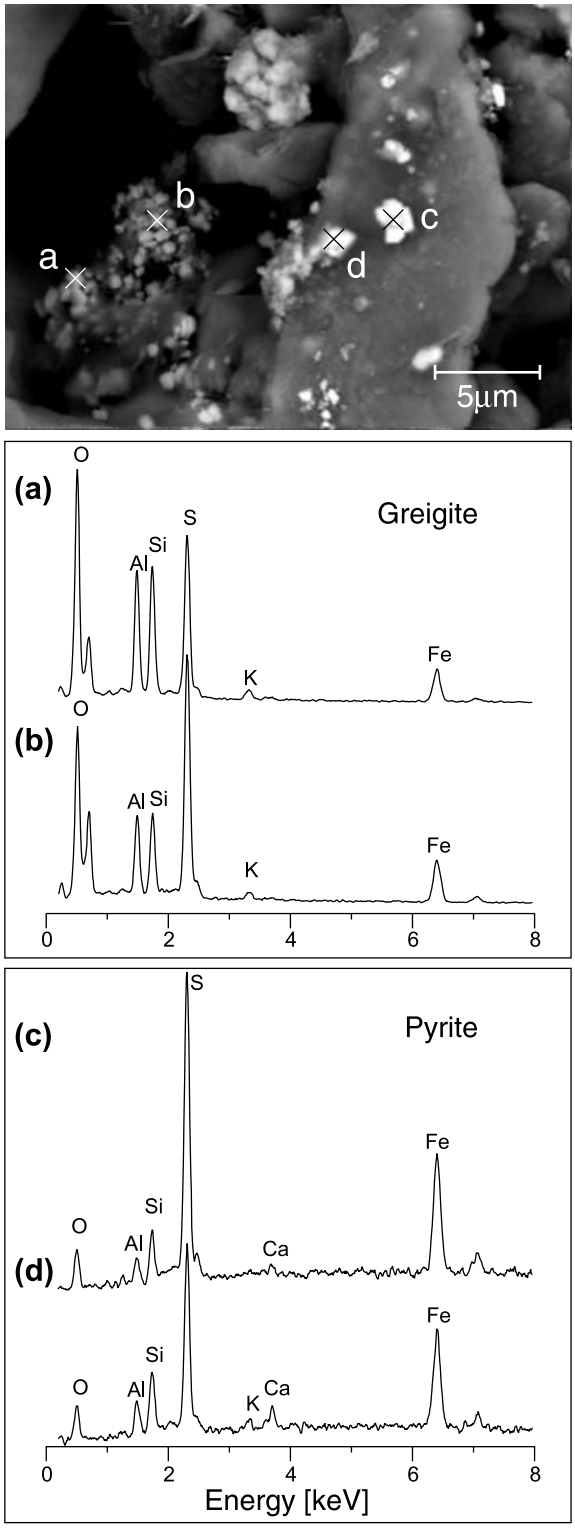

Figure 7. Backscattered electron micrograph of a dispersed magnetic extract from sample BD115. Clusters of fine-grained greigite (a and b) with individual grain sizes <50 nm. Grains c and d are pyrite particles with an average grain size of 2 μm. The respective elemental spectra are shown below; a cross on the micrograph marks the exact position of the EDS analysis. See also the caption for Fig. 6.

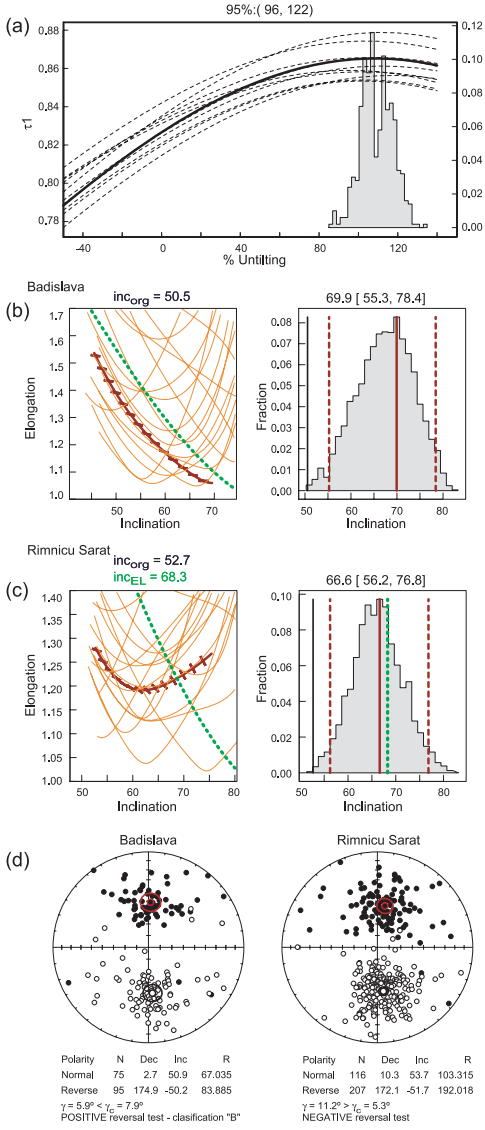

Figure 8. (a) Bootstrap fold test of Tauxe & Watson (1994), applied to both normal and reversed polarity characteristic remanent magnetization (ChRM) directions. Variation of the principal eigenvector τ_1 with percentage of unfolding is depicted as a solid line; dashed lines are bootstrap examples. The distribution of the maxima of τ_1 is shown by the histogram. The 95 per cent confidence interval (96–122 per cent) includes the 100 per cent unfolding orientation, which supports a pre-folding magnetization. Panels b and c contain elongation—inclination plots upon flattening for Badislava and Rîmnicu Sărat, respectively, following the field model TK03.GAD of Tauxe & Kent (2004). On the left-hand side: thick red line = inclination from the data set, red barbed lines = elongation direction, green dotted line = model, thin lines = examples of bootstraps. The inclination most consistent with the TK03.GAD model is the intersection with the model (green dotted line). On the right-hand side the distribution resulting from 5000 bootstraps is given, including the most frequent inclination (thick red line) and the model (the green dotted line). The 95 per cent confidence limit is shown in grey shading. The inclination of the original data set (black line) is significantly lower than the 95 per cent confidence interval. (d) Equal area projection of ChRM directions in tilt-corrected coordinates for the samples marked with green dots from the Badislava and Rîmnicu Sărat records in Fig. 1. Solid (open) circles indicate normal (reversed) polarity. The reversal test is positive for Badislava (classification B according to McFadden & McElhinny (1990), with the angle γ between the normal and reversed polarities smaller than the critical angle γ_c. The reversal test is negative for the Rîmnicu Sărat section.

indicates a dominant magnetic carrier with $B_{1/2}$ = 76.7–78.5 mT and a low dispersion DP = 0.14 in all three analysed samples (Figs 10g–i). Again, these values are close to those for samples TP 57 and RR 025 (Figs 5b and c) and to a large number of other samples (Table 2).

6.3 Environmental implications

A change in magnetic properties is observed in the sedimentary successions of both the southern and eastern Carpathian foredeep during the Lower Pontian, where the main carrier of the palaeomagnetic signal changed from magnetite to dominantly greigite (Fig. 1). Major tectonic events in the Paratethys and Mediterranean regions reshaped the local and regional basin configuration at the same time, which drastically influenced palaeoenvironmental conditions. It is useful to explore the palaeoenvironmental conditions that were responsible for the formation of palaeomagnetically stable greigite in the Carpathian foredeep.

During Miocene–Pliocene times, the Carpathian foredeep was part of the Eastern Paratethys, which was a large brackish to freshwater lake that was more or less restricted from the global ocean system. The Carpathian foredeep sediments were deposited in a high-energy environment (close to the shoreline) and their micro and macrofaunal contents are substantial. The presence of benthic ostracods (Olteanu 1995) and molluscs (Papaianopol 1995) throughout the entire upper Miocene–Pliocene time interval demonstrates that the lowermost water column remained sufficiently oxygenated for these organisms to live. Anoxic conditions favouring greigite formation could, therefore, only have been present within the sediments, probably related to degradation of organic matter during rapid burial.

In the Sarmatian-Meotian parts of the sections (∼9–6 Ma), high-energy brackish to marine conditions probably led to oxygenation of the uppermost sediment column. Detrital magnetite was, therefore, not reductively dissolved; it remained the main carrier of the detrital remanent magnetization. The majority of the samples from these parts of the eastern Carpathian sequences have high NRM intensities and low-field susceptibilities (at least two orders of magnitude higher than the greigite-dominated parts of the section). This is presumably related to reworked volcaniclastic input, which supplied additional magnetic material to the basin (Panaiotu *et al.* 2007). Sediment provenance analyses indicate that there was, during Chron C3r, a major switch in the main source area for the foredeep basin from an active volcanic arc towards an orogenic belt composed of metamorphic and sedimentary deposits (Panaiotu *et al.* 2007). In the eastern Carpathian foredeep, this event coincided with a major change in subsidence and accumulation rate, from 0.60 to 1.55 m kyr^{-1} (Vasiliev *et al.* 2004). In the southern Carpathian foredeep, the magnetostratigraphic records are not long enough to determine representative sediment accumulation curves (Vasiliev *et al.* 2005).

In addition, it is noteworthy that the Mediterranean Messinian Salinity Crisis completely occurred within Chron C3r (Gautier *et al.* 1994; Krijgsman 2002). A significant base level drop in the Mediterranean could have easily changed water circulation patterns within the Eastern Paratethys and also could have affected the local climate system. In this scenario, however, one would expect the original conditions to have been re-established when the Mediterranean refilled at the Miocene–Pliocene boundary. Further research is necessary to fully understand the causes and consequences of the interactive dynamics of these two water masses at that time. Nevertheless, it has often been suggested that the desiccation of the

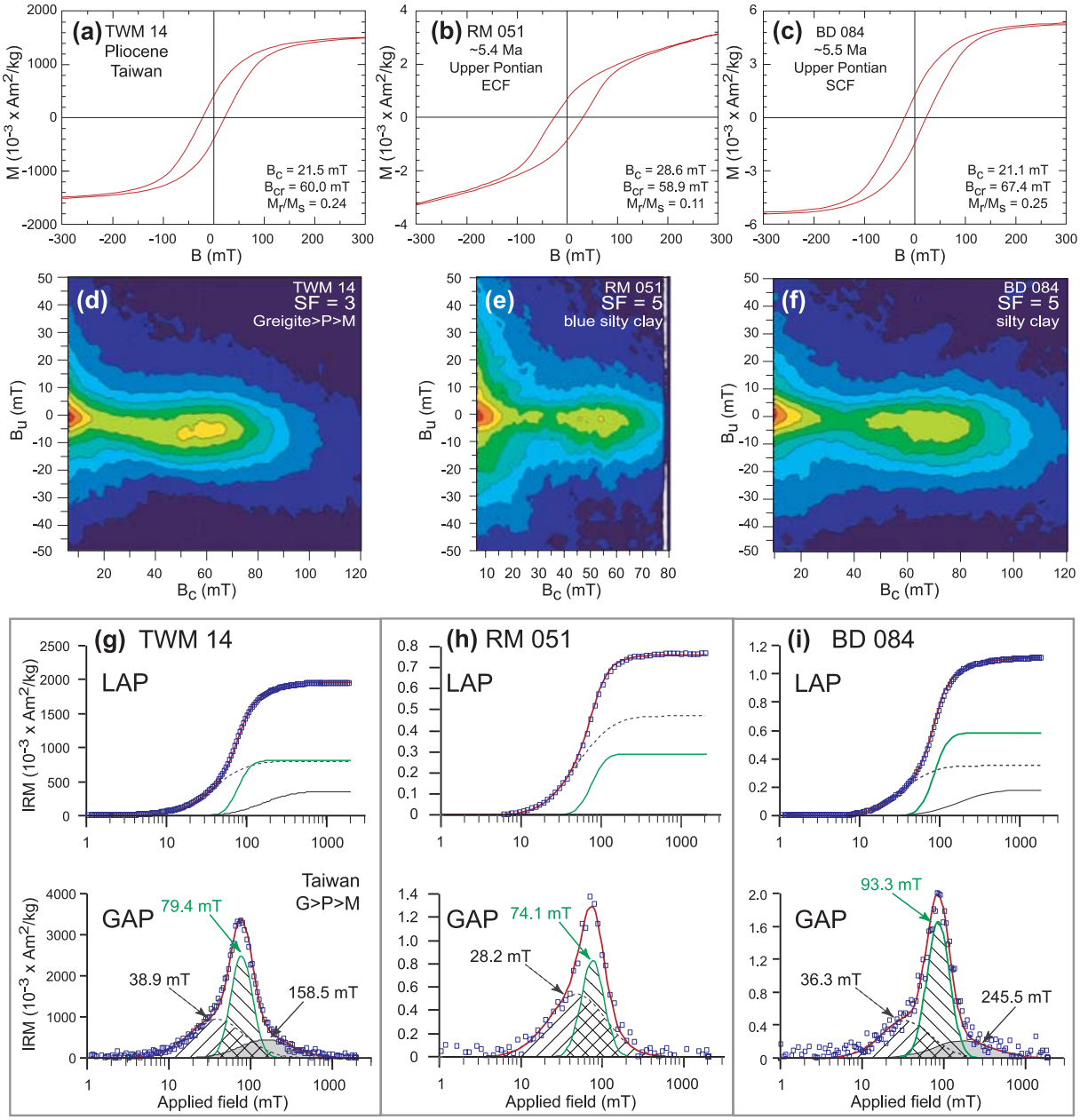

Figure 9. Hysteresis loops, FORC diagrams and IRM component analysis for a magnetic concentrate TWM 14 (panels a, d and g) from Pliocene–Pleistocene sedimentary rocks in Taiwan and for Carpathian foredeep bulk samples RM 051 (panels b, e and h) and BD 084 (panels c, f and i), respectively. See also captions for Figs 3 and 4.

Mediterranean also extended into the Paratethys region since seismic profiles of the Black Sea basin show clear evidence of canyon cutting (Hsü & Giovanoli 1979; Gillet *et al.* 2003; Dinu *et al.* 2005) and Gilbert-type deltas are observed along the gorges of the Danube river at the Romanian–Serbian border (Clauzon *et al.* 2005).

It is clear that greigite formation in the Romanian Carpathian foredeep palaeoenvironment occurred in a high sedimentation rate setting. This situation is similar to the palaeoenvironmental settings of south-western Taiwan (Horng *et al.* 1992a,b, 1998, Jiang *et al.* 2001; Kao *et al.* 2004) and of eastern New Zealand (Roberts & Turner 1993; Rowan & Roberts 2006). High sedimentation rates along with rapid burial of organic matter will lead to a completely anoxic diagenetic environment within a metre of the sediment/water interface (Westrich & Berner 1984; Canfield & Berner 1987). In such settings, the greigite in the Eastern Carpathian foredeep could have formed during early diagenesis, within 1000 yr of deposition (at sedimentation rates >1 m kyr^{-1}). Such a delay ($\sim$1000 yr) between sediment deposition and NRM acquisition is insignificant for most of palaeomagnetic studies and is certainly acceptable for magnetostratigraphic dating.

7 CONCLUSIONS

Rock magnetic analyses and SEM observations indicate that the magnetic signal in the Romanian Carpathian foredeep is carried by the iron sulphide, greigite. It is always found in the younger (Uppermost Miocene and Pliocene) parts of the sections. The greigite appears to have formed during early diagenesis, within 1000 yr of

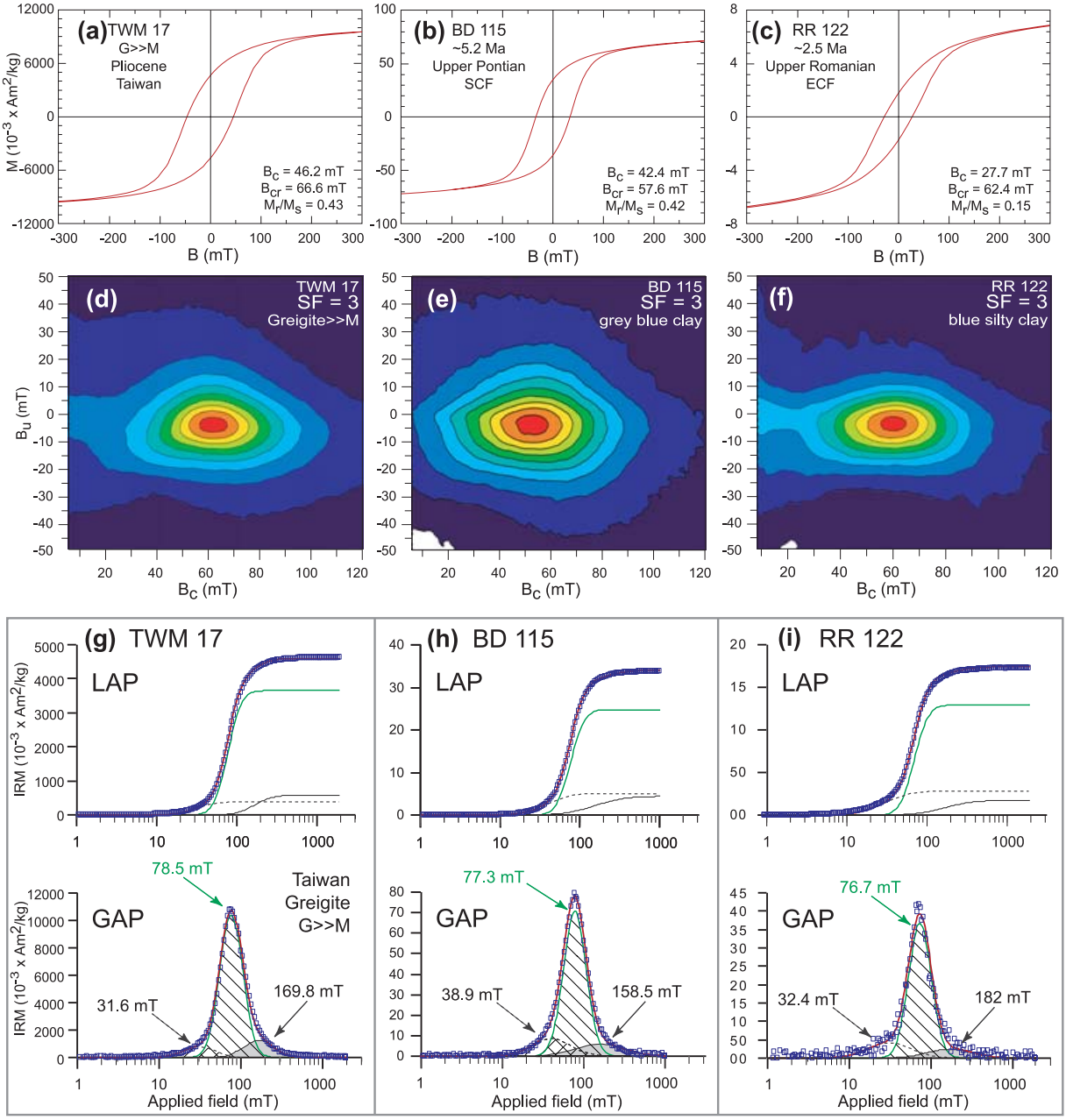

Figure 10. Hysteresis loops, FORC diagrams and IRM component analysis for a magnetic concentrate TWM 17 (panels a, d and g) from Pliocene–Pleistocene sedimentary rocks in Taiwan and for Carpathian foredeep bulk samples BD 115 (panels b, e and h) and RR 122 (panels c, f and i), respectively. See also the caption for Figs 3, 4 and 9.

deposition of the sediments. Greigite formation was related to rapid sedimentation and burial of organic matter, similar to other greigite-bearing environments in Taiwan and New Zealand.

The change in the dominant magnetic carrier from iron oxides to greigite coincides with a change in the accumulation rate in the eastern Carpathians when the sedimentary environment became anoxic. The appearance of greigite in Chron C3r (between 6.0 and 5.5 Ma) is most likely related to regional tectonic and/or climatic events that reshaped the basin configuration and consequently drastically influenced the palaeoenvironmental conditions. Biostratigraphic studies indicate that the lowermost water column remained well ventilated and sufficiently oxygenated throughout the entire succession, therefore, we conclude that the anoxic conditions favouring greigite formation could only have been present within the sediments, probably related to degradation of organic matter during rapid but shallow burial.

ACKNOWLEDGMENTS

This work was financially supported by the Netherlands Research Centre for Integrated Solid Earth Sciences (ISES). We thank Marius, Cristina, Gabi, Cristian, Guillaume and Liliana for their help in the field. Special thanks to Fatima Martín Hernández for helpful discussions and to Ramon Egli for carrying out his type of analyses. Dr C. S. Horng kindly provided greigite-bearing samples from

Taiwan. The comments of Andrew Roberts and an anonymous reviewer significantly improved the manuscript.

REFERENCES

Berner, R.A., 1984. Sedimentary pyrite formation: An update, *Geochim. Cosmochim. Acta,* **48,** 605–615.

Canfield, D.E. & Berner, R.A., 1987. Dissolution and pyritization of magnetite in anoxic marine sediments, *Geochim. Cosmochim. Acta,* **51,** 645–659.

Clark, D.A., 1984. Hysteresis properties of sized dispersed monoclinic pyrrhotite grains, *Geophys. Res. Lett.,* **11,** 173–176.

Clauzon, G., Suc, J.-P., Popescu, S.-P., Marunteanu, M., Rubino, J.-L., Marinescu, F. & Melinte, M.C., 2005. Influence of the Mediterranean sea-level changes on the Dacic Basin (Eastern Paratethys) during the late Neogene: the Mediterranean Lago Mare facies deciphered, *Basin Res.,* **17,** 437–462.

Cloetingh, S., Matenco, L., Bada, G., Dinu, C. & Mocanu, V., 2005. The evolution of the Carpathians–Pannonian system: interaction between neotectonics, deep structure, polyphase orogeny and sedimentary basins in a source to sink natural laboratory, *Tectonophysics,* **410,** 1–14.

Dekkers, M.J., 1988a. Magnetic properties of natural pyrrhotite. I. Behaviour of initial susceptibility and saturation magnetization-related rock magnetic parameters in a grain-size-dependent framework, *Phys. Earth Planet. Inter.,* **52,** 376–393.

Dekkers, M.J., 1988b. Some rockmagnetic parameters for natural goethite, pyrrhotite and fine-grained hematite, *PhD thesis*, Utrecht University, Utrecht.

Dekkers, M.J., Passier, H.F. & Schoonen, M.A.A., 2000. Magnetic properties of hydrothermally synthesized greigite (Fe_3S_4)-II. High- and low-temperature characteristics, *Geophys. J. Int.,* **141,** 809–819.

Dinarès-Turell, J. & Dekkers, M.J., 1999. Diagenesis and remanence acquisition in the Lower Trubi marls at Punta di Maiata (southern Sicily): paleomagnetic and rock magnetic observations, in *Paleomagnetism and Diagenesis in Sediments*, Vol. **151,** pp. 53–69, eds Tarling, D.H. & Turner, P., Geol. Soc. Lond. Spec. Publ., London.

Dinu, C., Wong, H.K., Tambrea, D. & Matenco, L., 2005. Stratigraphic and structural characteristics of the Romanian Carpathians, *Tectonophysics,* **410,** 417–435.

Dupont-Nivet, G., Vasiliev, I., Langereis, C.G., Krijgsman, W. & Panaiotu, C., 2005. Neogene tectonic evolution of the southern and eastern Carpathians constrained by paleomagnetism, *Earth Planet. Sci. Lett.,* **236,** 234–387.

Egli, R., 2004a. Characterisation of individual rock magnetic components by analysis of remanence curves, 1. Unmixing natural sediments, *Stud. Geophys. Geodaet.,* **48,** 391–446.

Egli, R., 2004b. Characterisation of individual rock magnetic components by analysis of remanence curves, 2. Fundamental properties of coercivity distribution, *Phys. Chem. Earth,* **29,** 851–867.

Gautier, F., Clauzon, G., Suc, J.-P., Cravatte, J. & Violanti, D., 1994. Age et durée de la crise de salinité Messinienne, *C. R. Acad. Sci. Paris*, **318,** 1103–1109.

Gillet, H., Lericolais, G., Rehault, J.-P. & Dinu, C., 2003. La stratigraphie Oligo-Miocene et la surface d'erosion Messinienne en Mer Noire, stratigraphie seismique haute resolution, *C. R. Geoscience,* **335,** 907–916.

Grasu, C., Miclaus, C., Catana, C. & Bobos, I., 1999. *Molasa Carpatilor Orientali*, pp. 227, Editura Tehnica, Bucharest.

Hallam, D.F. & Maher, B.A., 1994. A record of reversed polarity carried by the iron sulphide greigite in British early Pleistocene sediments, *Earth Planet. Sci. Lett.,* **121,** 71–80.

Heslop, D., McIntosh, G. & Dekkers, M.J., 2004. Using time-and temperature-dependent Preisach models to investigate the limitations of modelling isothermal remanent magnetization acquisition curves with cumulative log Gaussian functions, *Geophys. J. Int.,* **157,** 55–63.

Horng, C.-S., Chen, J.-C. & Lee, T.-Q., 1992a. Variation in the magnetic minerals from two Plio-Pleistocene marine-deposited sections, southwestern Taiwan, *J. Geol. Soc. China,* **35,** 323–335.

Horng, C.-S., Laj, C., Lee, T.-Q. & Chen, J.-C., 1992b. Magnetic characteristics of sedimentary rocks from the Tsengwen-chi and Erhjen-chi sections in southwestern Taiwan, *TAO,* **3,** 519–532.

Horng, C.-S. & Roberts, A.P., 2006. Authigenic or detrital origin of pyrrhotite in sediments?: Resolving a paleomagnetic conundrum, *Earth Planet. Sci. Lett.,* **241,** 750–762.

Horng, C.-S., Torii, M., Shea, K.-S. & Kao, S.-J., 1998. Inconsistent magnetic polarities between greigite- and pyrrhotite/magnetite-bearing marine sediments from the Tsailiao-chi section, southwestern Taiwan, *Earth Planet. Sci. Lett.,* **164,** 467–481.

Hsü, K.J. & Giovanoli, F., 1979. Messinian event in the Black Sea, *Palaeogeogr. Palaeoclimatol. Palaeoecol.,* **29,** 75–93.

Jiang, W.-T., Horng, C.-S., Roberts, A.P. & Peacor, D.R., 2001. Contradictory magnetic polarities in sediments and variable timing of neoformation of authigenic greigite, *Earth Planet. Sci. Lett.,* **193,** 1–12.

Jørgensen, B.B., Böttcher, M.E., Luschen, H., Neretin, L.N. & Volkov, I.I., 2003. Anaerobic methane oxidation and the deep H_2S sink generate isotopically heavy sulphides in Black Sea sediments, *Geochim. Cosmochim. Acta,* **68,** 2095–2118.

Kao, S.-J., Horng, C.-S., Roberts, A.P. & Liu, K.-K., 2004. Carbon-sulfur-iron relationships in sedimentary rocks from souwthwestern Taiwan: influence of geochemical environment on greigite and pyrrhotite formation, *Chem. Geol.,* **203,** 153–168.

Krijgsman, W., 2002. The Mediterranean: mare nostrum of earth sciences, *Earth Planet. Sci. Lett.,* **205,** 1–12.

Krijgsman, W. & Tauxe, L., 2004. Shallow bias in Mediterranean paleomagnetic directions caused by inclination error, *Earth Planet. Sci. Lett.*, **222,** 685– 695.

Krs, M., Novak, F., Krsova, M., Pruner, P., Koulikova, L. & Jansa, J., 1992. Magnetic properties and metastability of greigite-smythite mineralization brown-coal basins of the Krusna Hory Piedmont, Bohemia, *Phys. Earth Planet. Inter.,* **70,** 273–287.

Kruiver, P.P., Dekkers, M.J. & Heslop, D., 2001. Quantification of the magnetic coercivity components by the analysis of acquisition curves of isothermal remanent magnetisation, *Earth Planet. Sci. Lett.,* **189,** 269–276.

Linssen, J.H., 1988. Preliminary results of a study of four successive sedimentary geomagnetic reversal records from the Mediterranean (Upper Thvera, Lower and Upper Sidufjall, and Lower Nunivak), *Phys. Earth Planet. Inter.,* **52,** 207–231.

Maher, B.A. & Hallam, D.F., 2005. Magnetic carriers and remanence mechanisms in magnetite-poor sediments of Pleistocene age, southern North Sea margin, *J. Quat. Sci.,* **20,** 79–94.

Mary, C., Iaccarino, S., Courtillot, V., Besse, J. & Aissaoui, D.M., 1993. Magnetostratigraphy of Pliocene sediments from the Stirone River (Po Valley), *Geophys. J. Int.,* **112,** 359–380.

Matenco, L., 1997. Tectonic evolution of the outer Romanian Carpathians: Constraints from kinematic analysis and flexural modeling, *PhD thesis*. Vrije Universiteit, Amsterdam.

McFadden, P.L. & McElhinny, M.W., 1990. Classification of the reversal test in palaeomagnetism, *Geophys. J. Int.,* **103,** 725–729.

Menyeh, A. & O'Reilly, W., 1991. The magnetization process in monoclinic pyrrhotite (Fe_7S_8) particles, *Geophys. J. Int.,* **104,** 387–399.

Mullender, T.A.T., van Velzen, A.J. & Dekkers, M.J., 1993. Continous drift correction and separate identification of ferromagnetic and paramagnetic contribution in thermomagnetic runs, *Geophys. J. Int.,* **114,** 663–672.

Newell, A.J., 2005. A high-precision model of first-order reversal curve (FORC) functions for single-domain ferromagnets with uniaxial anisotropy, *Geochem. Geophys. Geosys.*, **6** Q05010, doi:, 1–13.

Olteanu, R., 1995. Dacian ostracodes, in *Chronostratigraphie und Neostratotypen*, pp. 530, Editura Academiei Romane, Bucharest.

Panaiotu, C.E., Vasiliev, I., Panaiotu, C.G., Krijgsman, W. & Langereis, C.G., 2007. Provenance analysis as a key of East Carpathians exhumation: evidence from Focsani Basin (Romania), *Terra Nova,* **19,** 120–126.

Papaianopol, I., 1995. Faune de mollusques daciens du Bassin Dacique, in *Chrostratigraphie und Neostratotypen*, pp. 530, Editute Academiei Romane, Bucharest.

Passier, H.F., de Lange, G.J. & Dekkers, M.J., 2001. Rock-magnetic properties and geochemistry of the active oxidation front and the youngest sapropel in the Mediterranean, *Geophys. J. Int.,* **145,** 604–614.

Peters, C. & Dekkers, M.J., 2003. Selected room temperature magnetic parameters as a function of mineralogy, concentration and grain size, *Phys. Chem. Earth,* **28,** 659–667.

Pike, C.R., Roberts, A.P. & Verosub, K.L., 1999. Characterizing interactions in fine magnetic particle systems using first-order reversal curves, *J. Appl. Phys.,* **85,** 6660–6667.

Rabagia, T. & Matenco, L., 1999. Tertiary tectonic and sedimentological evolution of the South Carpathians foredeep: tectonic vs eustatic control, *Mar. Petrol. Geol.,* **16,** 719–740.

Reynolds, R.L., Tuttle, M.L., Rice, C.A., Fishman, N.S., Karachewski, J.A. & Sherman, D.M., 1994. Magnetization and geochemistry of greigite bearing Cretaceous strata, North Slope Basin, Alaska, *Am. J. Sci.,* **294,** 485–528.

Roberts, A.P., 1995. Magnetic properties of sedimentary greigite (Fe_3S_4), *Earth Planet. Sci. Lett.,* **134,** 227–236.

Roberts, A.P., Cui, Y.L. & Verosub, K.L., 1995. Wasp-waisted hysteresis loops: Mineral magnetic characteristics and discrimination of components in mixed magnetic systems, *J. Geophys. Res.,* **100,** 17 909–179 24.

Roberts, A.P., Pike, C.R. & Verosub, K.L., 2000. First-order reversal curve diagrams: a new tool for characterizing the magnetic properties of natural samples, *J. Geophys. Res.,* **102,** 28 461–28 475.

Roberts, A.P. & Turner, G.M., 1993. Diagenetic formation of ferrimagnetic iron sulphide minerals in rapidly deposited marine sediments, South Island, New Zealand, *Earth Planet. Sci. Lett.,* **115,** 257–273.

Roberts, A.P. & Weaver, R., 2005. Multiple mecanisms of remagnetization involving sedimentary greigite (Fe_3S_4), *Earth Planet. Sci. Lett.,* **231,** 263–277.

Roberts, A.P., Liu, Q.S., Rowan, C.J., Chang, L., Carvallo, C., Torrent, J. & Horng, C.S., 2006. Characterization of hematite (alpha-Fe_2O_3), goethite (alpha-FeOOH), greigite (Fe_3S_4), and pyrrhotite (Fe_7S_8) using first-order reversal curve diagrams, *J. Geopys. Res.*, **111,** B12535, doi:.

Ross, D.A. & Degens, E.T., 1974. Recent sediments of the Black Sea, *Geochem. Biol.,* **20,** 183–199.

Rowan, C.J. & Roberts, A.P., 2006. Magnetite dissolution, diachronous greigite formation, and secondary magnetizations from pyrite oxidation: unravelling complex magnetizations in Neogene marine sediments from New Zealand, *Earth Planet. Sci. Lett.,* **241,** 119–137.

Sagnotti, L., Roberts, A.P., Weaver, R., Verosub, K.L., Florindo, F., Pike, C.R., Clayton, T. & Wilson, G.S., 2005. Apparent magnetic polarity reversals due to remagnetization resulting from late diagenetic growth of greigite from siderite, *Geophys. J. Int.,* **160,** 89–100.

Sandulescu, M., 1984. *Geotectonica Romaniei*, pp. 450, Editura Tehnica, Bucharest.

Sandulescu, M., 1988. Cenozoic tectonic history of the Carpathians, *The Pannonian Basin, a Study in Basin Evolution, AAPG Memoir,* **28,** 17–25.

Snowball, I.F., 1991. Magnetic hystereis properties of greigite (Fe_3S_4) and a new occurrence in Holocene sediments from Swedish Lappland, *Phys. Earth Planet. Inter.,* **38,** 32–40.

Stoica, M., Lazar, I., Vasiliev, I. & Krijgsman, W., 2007. Mollusc assemblages of the Pontian and Dacian deposits in the Topolog-Arges area (southern Carpathian foredeep - Romania), *Geobios,* **40,** 319–405.

Tarapoanca, M., 2003. Architecture of the Focsani Depression: a 13 km deep basin in the Carpathians bend zone (Romania), *Tectonics,* **22,** 13-1–13-17.

Tauxe, L. & Kent, D.V., 2004. A new statistical model for the geomagnetic field and the detection of shallow bias in paleomagnetic inclinations: was the ancient magnetic field dipolar?, in *Opdyke Chapman Conference: Timescales of the Paleomagnetic Field*, Gainesville, AGU Geophys. Monogr. Series **145,** pp. 328, eds Channell, J. E.T., Kent, D.V., Lowrie, W. & Meert, J.G., Am. geophys. Un. Monogr., Washington, DC.

Tauxe, L., Mullender, T.A.T. & Pick, T., 1996. Potbellies, wasp-waists, and superparamagnetism in magnetic hysteresis, *J. Geophys. Res.,* **101,** 571–583.

Tauxe, L. & Watson, G.S., 1994. The fold test: an eigen analysis approach, *Earth Planet. Sci. Lett.,* **122,** 331–341.

Tric, E., Laj, C., Jehanno, C., Valet, J.-P., Kissel, C., Mazaud, A. & Iaccarino, S., 1991. High-resolution record of the Upper Olduvai transition from Po Valley (Italy) sediments: support for dipolar transition geometry?, *Phys. Earth Planet. Inter.,* **65,** 319–336.

Vasiliev, I., Krijgsman, W., Langereis, C.G., Panaiotu, C.E., Matenco, L. & Bertotti, G., 2004. Towards an astrochronological framework for the eastern Paratethys Mio-Pliocene sedimentary sequences of the Focsani basin (Romania), *Earth Planet. Sci. Lett.,* **227,** 231–247.

Vasiliev, I., Krijgsman, W., Stoica, M. & Langereis, C.G., 2005. Mio-Pliocene magnetostratigraphy in the southern Carpathian foredeep and Mediterranean-Paratethys correlation, *Terra Nova,* **17,** 374–387.

Weaver, R., Roberts, A.P. & Barker, A.J., 2002. A late diagenetic (syn-folding) magnetization carried by pyrrhotite: implications for paleomagnetic studies of magnetic iron sulphide-bearing sediments, *Earth Planet. Sci. Lett.,* **200,** 371–386.

Westrich, J.T. & Berner, R.A., 1984. The role of sedimentary organic matter in bacterial sulphate reduction: the G model tested, *Limnol. Oceanogr.,* **29,** 236–249.